Crystallization of Very Low Density Copolymers of Ethylene with α-Olefins

J. MINICK,[1,*] A. MOET,[1,†] A. HILTNER,[1,‡] E. BAER,[1] and S. P. CHUM[2]

[1]Department of Macromolecular Science and Center for Applied Polymer Research, Case Western Reserve University, Cleveland, Ohio 44106; [2]Polyolefins & Elastomers Research, The Dow Chemical Company, Freeport, Texas 77541

SYNOPSIS

Differential scanning calorimetry (DSC) was used to analyze the crystal distribution in homogeneous ethylene–octene copolymers polymerized by the constrained geometry catalyst technology (CGCT). To minimize ambiguities from thermal history effects, copolymers were isothermally annealed at temperatures within the melting range. The cumulative crystallinity was related to the crystal distribution by the Gibbs–Thomson equation. The results provided a clear distinction between Type I copolymers (density less than 0.89 g/cc) and Type II copolymers (densities between 0.89 and 0.91 g/cc). The former had a single-crystal population that was identified with the bundled crystals seen in transmission electron micrographs. In comparison, the latter had two crystal populations that correlated with lamellar crystals and bundled crystals. © 1995 John Wiley & Sons, Inc.

INTRODUCTION

Recently, using Dow's INSITE® constrained geometry catalyst technology (CGCT), homogeneous ethylene copolymers were synthesized with fairly narrow molecular weight distribution.[1] In contrast, conventional heterogeneous multisite catalysts yield linear low-density polyethylenes (LLDPEs) with broad molecular weight and comonomer distributions. The control of molecular architecture afforded by the new catalysts makes it possible to produce homogeneous copolymers with crystallinities considerably lower than those of conventional LLDPEs or that can be obtained by fractionation of conventional LLDPEs.[2,3]

The ethylene–octene CGCT copolymers have been characterized as a function of comonomer content at constant molecular weight over a wide range of densities.[4] The polymers present a broad range of solid-state structures, from the highly crystalline, lamellar morphology of the homopolymer to the granular morphology of low crystallinity copolymers. As the comonomer content increases, the accompanying tensile behavior changes from necking and cold drawing typical of a semicrystalline thermoplastic to uniform drawing and high recovery characteristic of an elastomer. Although changes in morphological features and tensile properties occur gradually with increasing comonomer content, the combined body of observations from melting behavior, morphology, yielding, and large-scale deformation suggests a classification scheme with four distinct categories. These are described in Figure 1.

Materials with densities higher than 0.93 g/cc, Type IV, exhibit lamellar morphology with well-developed spherulitic superstructure. Type III polymers with densities between 0.93 and 0.91 g/cc have thinner lamellae and smaller spherulites. With increasing comonomer content, the spherulites are smaller and the lamellae are less ordered. Type II materials with densities between 0.91 and 0.89 g/cc have a mixed morphology of small lamellae and bundled crystals. Under favorable conditions, these materials form very small spherulites. Type I copolymers with densities less than 0.89 g/cc have no lamellae or spherulites. Fringed micellar or bundled crystals are inferred from the low degree of crystallinity, the low melting temperature, and the granular, nonlamellar morphology.[5]

* Present address: The Dow Chemical Co., Freeport, TX.
† Present address: Department of Chemical and Petroleum Engineering, United Arab Emirate University, Al-Ain, UAE.
‡ To whom correspondence should be addressed.

Journal of Applied Polymer Science, Vol. 58, 1371–1384 (1995)
 CCC 0021-8995/95/081371-14

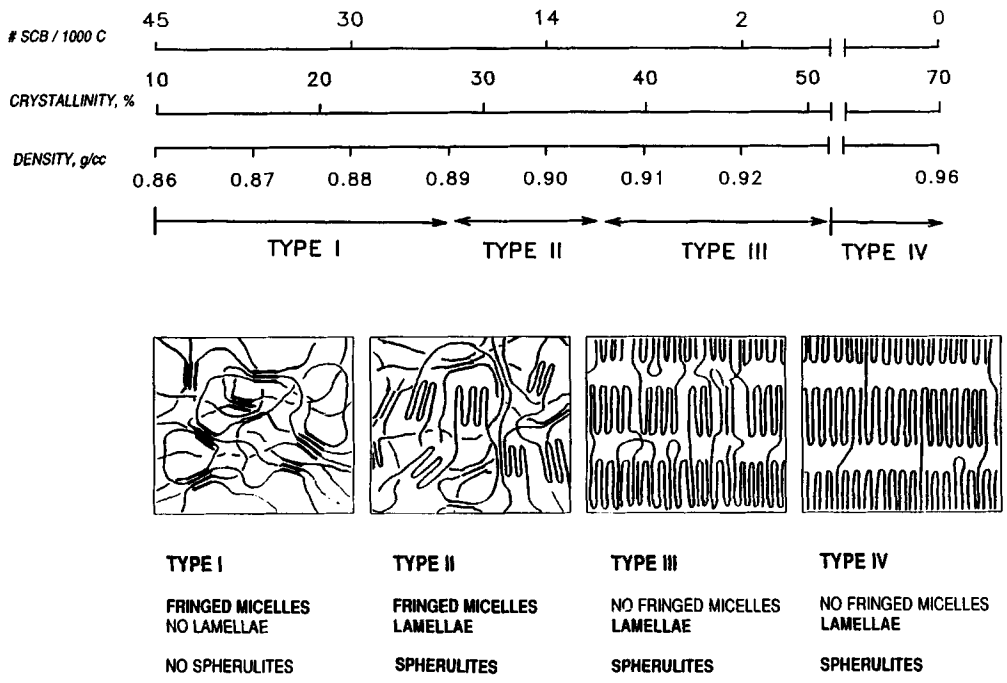

Figure 1 Schematic illustration of the four types of CGCT polymers as defined in Ref. 4.

Very broad differential scanning calorimetry (DSC) melting endotherms that may extend over a 100°C temperature range are typical of the CGCT copolymers. The onset of melting occurs near ambient temperature for even the higher-density copolymers and the melting range begins at subambient temperatures for the low-density, Type I copolymers. At least in part, the broad melting endotherms of copolymers are a consequence of chain heterogeneity. The distribution in length of crystallizable ethylene sequences, imposed by the placement of noncrystallizable comonomer units along the chain, is responsible for a broad distribution of crystal sizes. The crystal-size distribution can change when the polymer is taken to a temperature above the onset of melting. This can occur by the melting of thinner crystals followed by recrystallization of any chain segments that are long enough to crystallize in thicker crystals. The potential also exists for the thinner crystals to thicken by chain segments sliding through the crystal. Because branches impede chains from moving easily through the crystal, copolymers with a high concentration of comonomer are not expected to undergo an increase in crystal thickness by this mechanism.

If comonomer units hinder recrystallization to a large extent, it is thought likely that there is a one-to-one correspondence between the crystal-size distribution and the melting temperature distribution.[6] Qualitative conclusions regarding the morphology can then be drawn from a DSC thermogram using, e.g., the Gibbs–Thomson equation.[7–10] However, the DSC melting thermograms of the CGCT copolymers suggest that this straightforward approach may not

Table I Copolymer Characteristics

Copolymer Designation	Pellet Density (g/cc)	Mol % Comonomer	SCB/1000C	I_2 (g/10 min)	I_{10}/I_2
CGCT9016-O	0.9014	2.4	12	0.9	8.8
CGCT8817-O	0.8879	4.7	25	0.9	8.7
CGCT87LMW-O	0.8751	n/a	n/a	80	n/a
CGCT8702-O	0.8724	6.0	32	0.8	8.1
CGCT8708-B	0.8746	7.5	41	1.0	7.4
CGCT863-O	0.8682	7.0	38	0.5	8
MIT88-B	0.8887	n/a	n/a	3.6	6
MIT88-P	0.8732	n/a	n/a	1.1	6

be used even with the lowest-density Type I copolymers. The single broad endothermic peak that characterizes melting of Type I copolymers immediately upon cooling from the melt is replaced by a double-melting peak after the copolymers have experienced ambient conditions for a period of time. That the new peak occurs just above ambient temperature is evidence that crystal morphology changes over time, perhaps by selective melting and recrystallization of the thinner, lower-melting crystals.

If crystals of Type I copolymers thicken or recrystallize during isothermal annealing, it is likely that the same thing happens to some extent during the DSC heating scan. The resulting thermogram is not easily interpreted. It is not possible, e.g., to relate the melting temperature to the crystal thickness unambiguously, nor does the crystal thickness distribution calculated from the DSC endotherm necessarily reproduce the crystal thickness distribution obtained in morphology studies at ambient temperature.[11,12] One procedure that has been used to correlate melting temperature with short-chain branching content has been to anneal in stages at decreasing temperatures starting from the melt.[13] An alternative approach to stagewise annealing, one that begins with the solid state and thus avoids nucleation effects, was used in the present study to obtain the crystal distribution in Types I and II CGCT copolymers. The copolymers were isothermally annealed at temperatures within the melting range. The subsequent heating scan was analyzed for relationships between the distribution of crystallizable ethylene sequences and the comonomer content, comonomer type, and molecular weight.

EXPERIMENTAL

Materials

Ethylene–octene copolymers and one ethylene–butene copolymer synthesized by the INSITE technology were provided by the Dow Chemical Co. in pellet form. The density range of the copolymers was 0.86–0.90 g/cc. The density, mol % comonomer, short-chain branch content (SCB), and melt flow index (I_2) of the copolymers are listed in Table I. The INSITE technology polymers are identified by the initials CGCT, the number following this designation is the density as provided by the manufacturer, and the comonomer is identified by O (octene) or B (butene). The density of the pellets was measured in an isopropanol–distilled water density column calibrated with glass floats. A minimum of four samples was analyzed to obtain the values given in Table I. The error in the measurement was ±0.0002 g/cc. Other information in Table I was provided by the Dow Chemical Co. Most of the CGCT copolymers have approximately the same molecular weight ($I_2 \approx 1$) except for one low molecular weight CGCT polymer ($I_2 = 80$). The melt flow index was measured at 190°C at loads of 10 and 2.16 kg (I_{10} and I_2, respectively). The I_{10}/I_2 ratio reflects the number of long-chain branches[14]; a value of 6 indicates virtually no long-chain branches, and the value for all the CGCT copolymers is about 8.

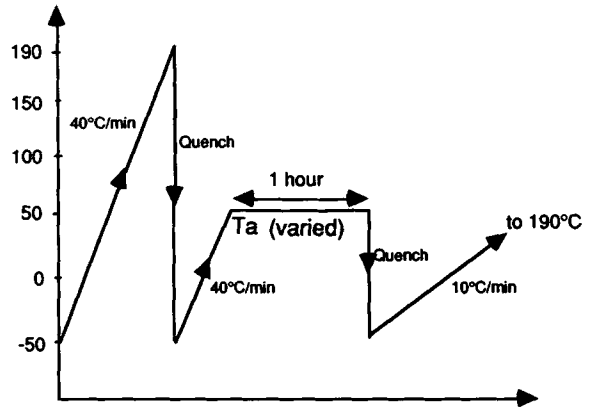

Figure 2 The thermal history used to obtain melting endotherms of annealed samples.

Copolymers of ethylene with propylene (MIT88-P) and butene (MIT88-B) were also obtained from Mitsui Petrochemicals Ltd. These were polymerized with a different catalyst system and, unlike the INSITE materials, do not have long-chain branches ($I_{10}/I_2 = 6$). The molecular weight of the butene copolymer ($I_2 = 3.6$) is slightly lower than that of the CGCT copolymers.

Plaques 1.1 mm thick were compression-molded from the pellets. The pellets were sandwiched between Mylar sheets, then heated at 190°C for 5 min under minimal pressure, followed by 5 min at 10,000 lbs and 1 min at 25,000 lbs. Samples were rapidly cooled by plunging the compression-molded plaque into ice water. Slowly cooled samples were made by allowing the plaque to cool from 190°C in the press at a rate of approximately 1°C/min.

Methods

Samples weighing between 5 and 10 mg were cut from the rapidly cooled plaques for thermal analysis. The copolymers were annealed at temperatures within the melting range according to the thermal history shown in Figure 2. The sample was heated to 190°C and quenched to −50°C before being heated to the annealing temperature where it was allowed

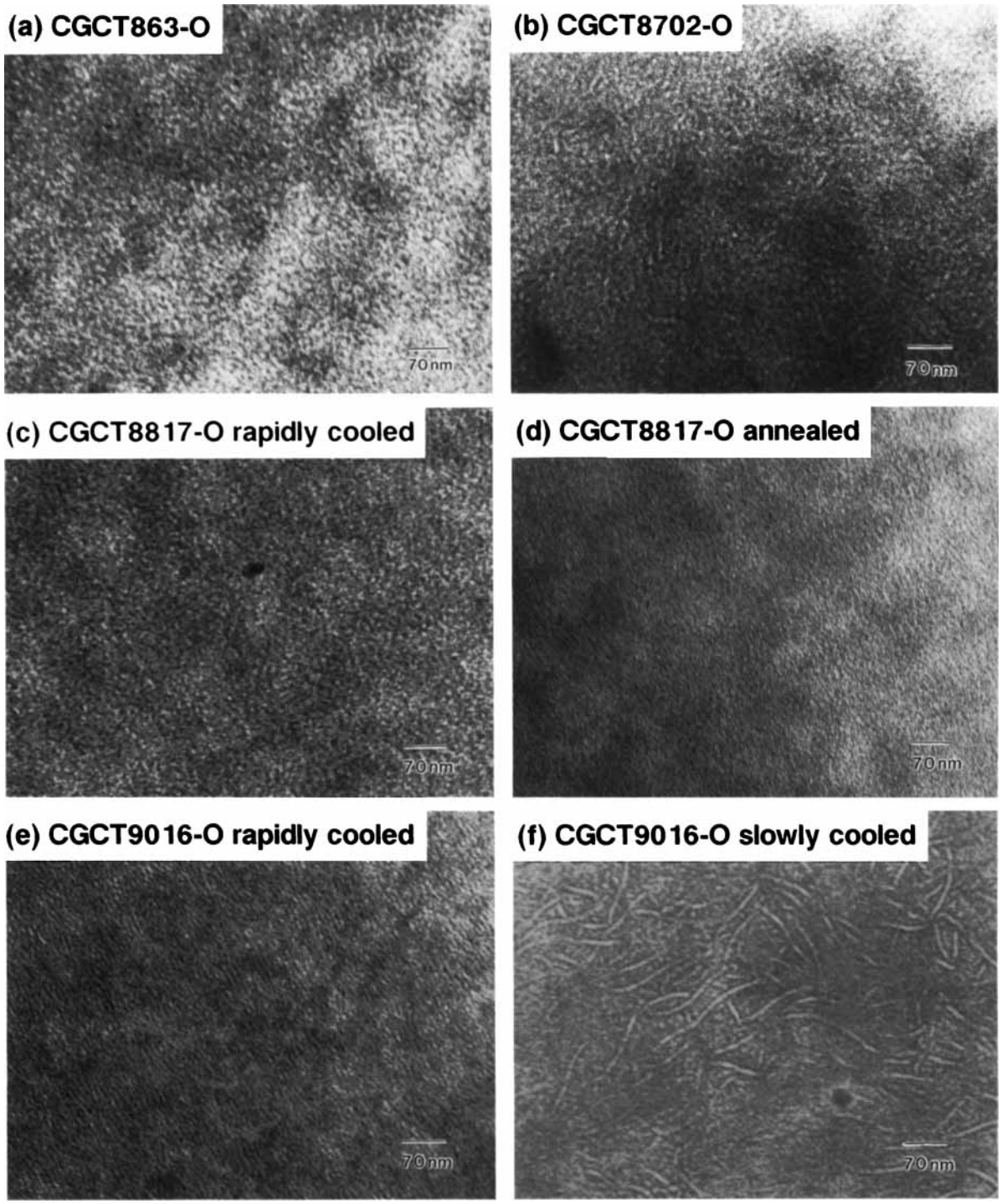

Figure 3 Micrographs of thin sections: (a) CGCT863–O rapidly cooled; (b) CGCT8702–O slowly cooled; (c) CGCT8817–O rapidly cooled; (d) CGCT8817–O annealed at 70°C for 1 h; (e) CGCT9016–O rapidly cooled; (f) CGCT9016–O slowly cooled.

to crystallize for 1 h. The sample was then cooled rapidly to −50°C and the subsequent thermogram was recorded. One sample was used for the entire series of annealing temperatures; when the series was complete, the sample was annealed again at 25°C to confirm that it had not degraded. All thermal analysis experiments were carried out in a Perkin-Elmer Model 7 DSC. Calculations of percent crystallinity were based on a heat of fusion of 290 J/g for the perfect crystal.[15]

Table II Copolymer Crystallinity and Melting Range

Copolymer	ΔH_m (J/g)	Crystallinity (%)	Melting Range (°C)
CGCT9016-O	95	33	25–110
CGCT8817-O	72	25	0–95
CGCT87LMW-O	45	15	< 0–85
CGCT8702-O	44	15	< 0–80
CGCT8708-B	43	15	< 0–80
CGCT863-O	34	12	< 0–70
MIT88B	73	25	0–95
MIT88P	47	16	< 0–65

Samples for electron microscopy were stained at room temperature for 2 h in a 0.2 g/10 mL solution of hydrated ruthenium chloride in sodium hypochlorite.[16] The samples were embedded in Hysol® epoxy resin from Dexter Electronic Materials Division; after the blocks were trimmed, the faces were stained in the vapor phase at 40°C and thin sections cut on an RMC MT6000-XL ultramicrotome with a CR-2000 cryosectioning unit. Copolymers with densities less than 0.90 g/cc were microtomed at −70°C to a thickness between 70 and 110 nm. The diamond knife was kept at −50°C. The trough fluid was a 60/40 wt/wt dimethylsulfoxide/water solution. The copolymer with a density of 0.90 was microtomed at room temperature to a thickness less than 100 nm. The sections were examined in a JEOL 100SX transmission electron microscope.

RESULTS AND DISCUSSION

Morphology of CGCT-O Copolymers

The morphologies of CGCT863-O (Type I), CGCT8702-O (Type I), CGCT8817-O (transitional from Type I to Type II), and CGCT9016-O (Type II) are shown in Figure 3. The CGCT863-O copolymer with 37 hexyl branches per 1000 carbon atoms in Figure 3(a) was rapidly cooled from the melt. The texture is uniformly granular. No lamellae are seen, but the granules are often aligned in beaded strings which are between 100 and 130 Å thick. Occasionally, the beaded strings are stacked in clusters of five or six strings. The unstained or lightly stained granules are assumed to be bundles of crystallized chain segments. Organization of the chain segments in these bundles may resemble the fringed micelle concept. The boundaries between the preferentially stained noncrystalline regions and the unstained granules are relatively diffuse, which suggests that the interfaces are not well ordered. Variations in surface order and crystalline bundle size could account for the wide temperature range over which these materials typically melt.

A thin section taken from a slowly cooled sample of CGCT8702-O with 32 hexyl branches per 1000 carbons is shown in Figure 3(b). The beaded strings are longer and more well defined than in CGCT863-O. They are approximately 75–100 Å thick, which is slightly thinner than in CGCT863-O. A few short segments of string are not beaded and resemble lamellar fragments. Micrographs of two CGCT8817-O samples, one rapidly cooled from the melt and the other annealed at 70°C, are shown in Figure 3(c) and (d). Both examples show beaded strings; the overall texture is finer in the annealed sample and the beaded strings have somewhat sharper boundaries. The 75–100 Å width of the strings is the same as in CGCT8702-O; however, there is more stacking of the beaded strings in CGCT8817-O than in the lower-density samples.

Morphological differences between CGCT8817-O with 25 hexyl groups per 1000 carbons and CGCT9016-O with 12 hexyls per 1000 carbons were evident. The thin section of the rapidly cooled sample of CGCT9016-O in Figure 3(e) contains many beaded strings approximately 75–100 Å thick. Many of the strings are stacked in large clusters. Alignment of the stacked strings provides an overall directionality to the morphology that was not apparent in the lower-density samples. There is also a clear effect of thermal history. The slowly cooled sample in Figure 3(f) has some long, curved lamellae with an average thickness of 140 Å. The edges of the lamellae are well defined, which indicates better surface order than in the beaded strings, with the possibility of some chain folding. Interspersed with the lamellae are short fragments of lamellae, beaded strings, and granules.

The appearance of well-defined lamellae in slowly cooled samples of CGCT9016-O suggests that this copolymer contains ethylene segments that are long enough to chain-fold. When rapidly cooled from the melt, the crystallizable chain segments are incor-

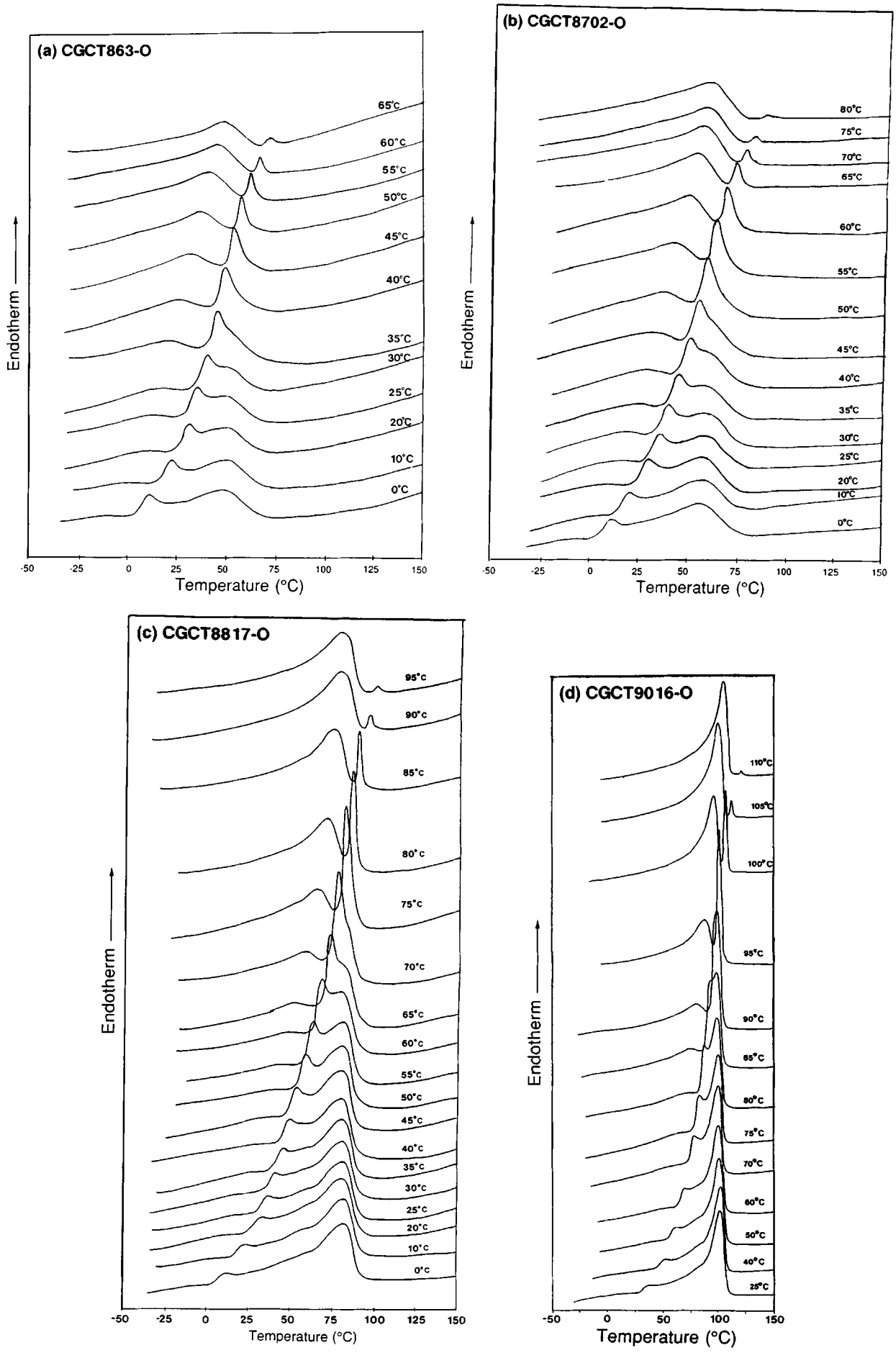
(a) CGCT863-O
65°C
60°C
55°C
50°C
45°C
40°C
35°C
30°C
25°C
20°C
10°C
0°C
Endotherm
-50 -25 0 25 50 75 100 125 150
Temperature (°C)
(b) CGCT8702-O
80°C
75°C
70°C
65°C
60°C
55°C
50°C
45°C
40°C
35°C
30°C
25°C
20°C
10°C
0°C
Endotherm
-50 -25 0 25 50 75 100 125 150
Temperature (°C)
(c) CGCT8817-O
95°C
90°C
85°C
80°C
75°C
70°C
65°C
60°C
55°C
50°C
45°C
40°C
35°C
30°C
25°C
20°C
10°C
0°C
Endotherm
-50 -25 0 25 50 75 100 125 150
Temperature (°C)
(d) CGCT9016-O
110°C
105°C
100°C
95°C
90°C
85°C
80°C
75°C
70°C
60°C
50°C
40°C
25°C
Endotherm
-50 0 50 100 150
Temperature (°C)

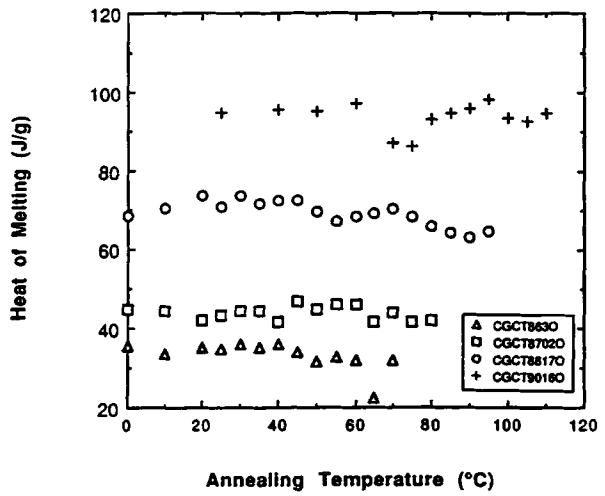

Figure 5 Total heat of melting ($\Delta H_{qc} + \Delta H_{ac}$) as a function of annealing temperature.

porated primarily into bundles and beaded strings, but during annealing or slow cooling, some can organize into more ordered lamallae. No annealing or cooling rate effects are observed in the morphology of the lower-density copolymers, although annealing effects are manifest as changes in the shape of the DSC melting endotherms. It is possible that even though the numerous branch points prevent the ethylene segments from being long enough to chain-fold to any significant extent, chain segments in the bundles may be able to reorganize during annealing or slow cooling to remove crystalline defects and improve surface order.

Melting Behavior of CGCT-O Copolymers

The CGCT copolymers typically have very broad melting endotherms that may extend over a 100°C temperature range (Table II). The melting range begins at subambient temperatures for the lowest-density copolymers; even for the higher-density copolymers, the onset of melting occurs near ambient temperature. Because of the broad melting range, there is ample opportunity for melting and recrystallization to occur during the DSC heating scan. If this is the case, the resulting melting thermogram is not easily interpreted. Samples were therefore annealed at a temperature within the melting range to allow the longer ethylene sequences to be incorporated into crystals with melting points above the annealing temperature. The sample was then rapidly cooled to crystallize the shorter ethylene sequences that were in the melt at the annealing temperature. The thermal history, including the subsequent heating scan of the annealed sample, is shown schematically in Figure 2.

A family of thermograms from a CGCT863-O sample that had been annealed at temperatures between 0 and 65°C is shown in Figure 4(a). Each thermogram consists of two or more endothermic peaks. The broad endothermic peak below T_a, the annealing temperature, is melting of the crystallizable chain segments that are in the melt at the annealing temperature and subsequently crystallize when the sample is cooled from the annealing temperature. Endotherms above T_a represent melting of crystals that are present at the annealing temperature. There is a relatively sharp endotherm just above T_a; in addition, especially with the lower annealing temperatures, there is a second broad endotherm above T_a at about 50°C. The temperature of this peak remains almost constant as the annealing temperature increases until the peak merges with the sharper, lower-temperature endotherm. The second endotherm above T_a is at least partially the result of dynamic melting and recrystallization during heating.[6]

Similar families of curves for the other three copolymers are also shown in Figure 4. Qualitatively, the thermograms exhibit similar features: a broad endotherm below T_a and, usually, two endotherms above T_a. The shapes of the thermograms for CGCT8702-O in Figure 4(b) are almost the same as for CGCT863-O, although for CGCT8702-O, the second endotherm above T_a is slightly larger and at a slightly higher temperature of 58°C compared to 54°C. The overall melting range is also very broad for CGCT8817-O [Fig. 4(c)] and CGCT9016-O [Fig. 4(d)]. The size and shape of the first endotherm above T_a is similar for all the copolymers. However, the heat content of the second endotherm above T_a, which is centered at 80°C for CGCT8817-O and 100°C for CGCT9016-O, increases as the number of short-chain branches decreases. It is possible that especially in CGCT9016-O the second peak represents melting of a distinct crystalline population superimposed on dynamic melting and recrystallization effects.[17]

The total heat of melting, plotted in Figure 5 for all four samples, does not vary with the annealing

Figure 4 Thermograms of annealed samples: (a) CGCT863-O; (b) CGCT8702-O; (c) CGCT8817-O; (d) CGCT9016-O. The annealing temperature (T_a) is indicated.

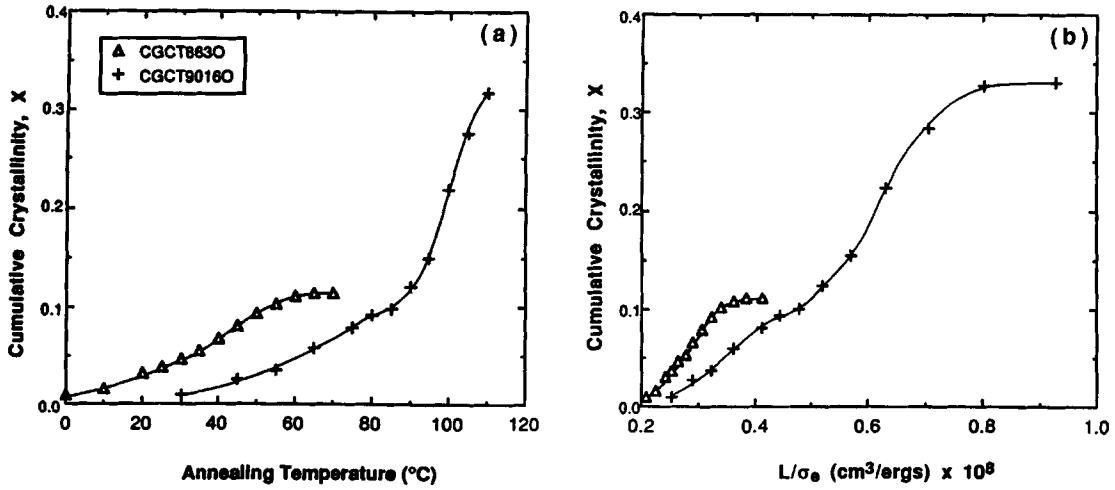

Figure 6 The cumulative crystallinity (**X**) as a function of (a) annealing temperature and (b) $\mathbf{L}/\sigma_e$ for CGCT863–O and CGCT9016–O.

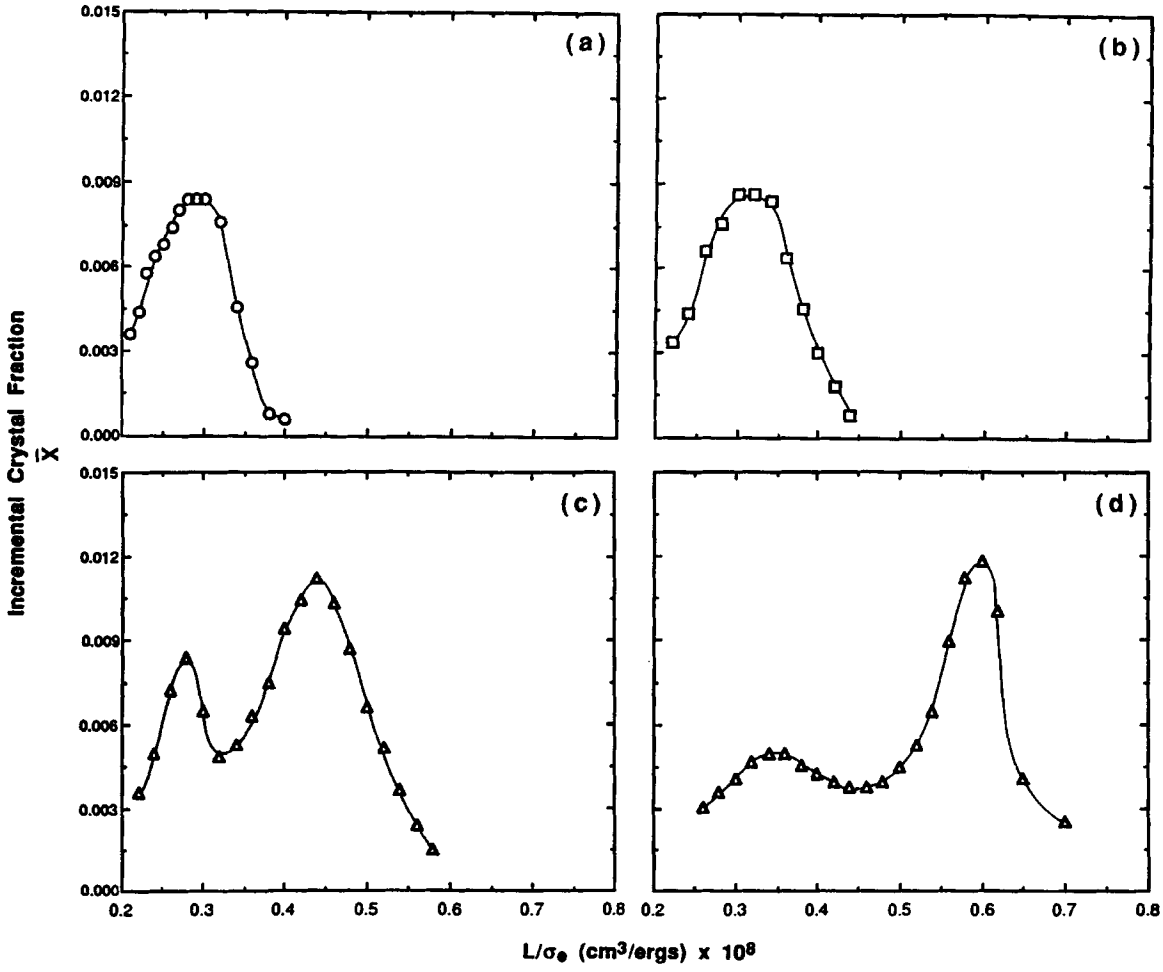

Figure 7 Incremental crystal fraction ($\bar{\mathbf{X}}$) of (a) CGCT863–O, (b) CGCT8702–O, (c) CGCT8817–O, and (d) CGCT9016–O.

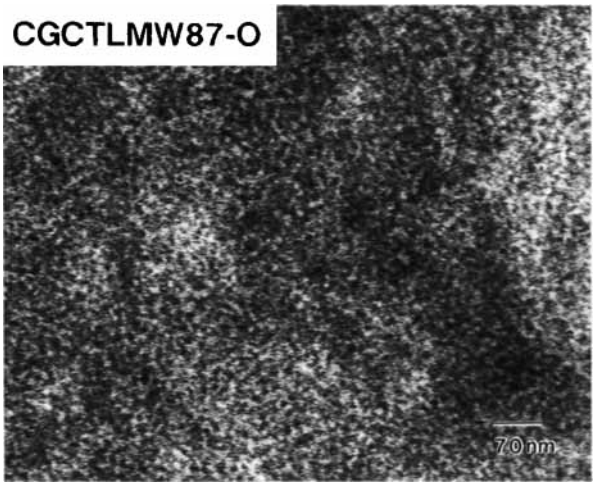

Figure 8 A thin section of rapidly cooled CGCTLMW87-O.

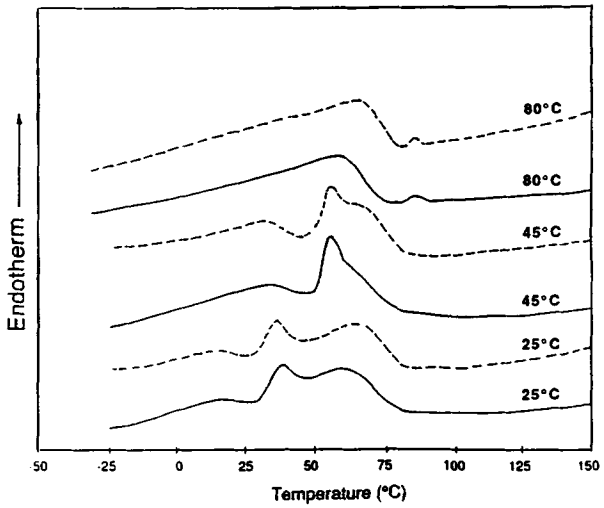

Figure 9 Selected thermograms of annealed (----) CGCTLMW87-O (I_2 = 80) and (———) CGCT8702-O (I_2 = 0.8). The annealing temperature (T_a) is indicated.

temperature. This indicates that the same population of chain segments crystallizes at each annealing temperature, although the crystal size and order vary. The average heat of melting increases from 34 J/g (±4 J/g) for CGCT863-O to 44 J/g (±3 J/g) for CGCT8702-O, 72 J/g (±7 J/g) for CGCT8817-O, and 95 J/g (±8 J/g) for CGCT9016-O.

The melting thermograms are divided into two regions above and below the annealing temperature. The heat of melting for the part below the annealing temperature (ΔH_{qc}) is assigned to melting of crystallizable chain segments with melting temperatures below the annealing temperature, and the heat of melting for the other part (ΔH_{ac}) represents melting of crystallizable chain segments with melting temperatures above the annealing temperature. The quantity ΔH_{qc} was normalized to the heat of fusion of the perfect crystal to obtain the cumulative crystallinity (**X**) which is plotted in Figure 6(a) as a function of annealing temperature for the copolymers with the lowest and the highest density. The curve for CGCT863-O has a fairly symmetrical S-shape. In contrast, the curve for CGCT9016-O is skewed. This may reflect a mixed population of crystal morphologies.

The melting temperature (T_m) is related to crystal size by the Gibbs-Thomson equation[18]:

$$\frac{T_m}{T_m^0} = 1 - \frac{2\sigma_e}{\mathbf{L}\Delta H_m^0} - \frac{\mathbf{C}\sigma_s}{\Delta H_m^0 \sqrt{\mathbf{va}}} \qquad (1)$$

where T_m^0 is the melting temperature of a polyethylene crystal of infinite thickness (415 K); ΔH_m^0, the heat of melting of the perfect crystal (290 J/g); **L**, the crystal thickness; **C**, a geometric factor relating perimeter to area; **v**, the number of chain segments in the cross section of the crystal; **a**, the cross-sectional area of one chain segment; σ_s, the lateral surface energy of a polyethylene crystal (9.6 erg/cm^2 [Ref. 19]); and σ_e, the surface energy which is on the order of 100 erg/cm^2 for regular folding.[20] The lateral surface energy term was initially considered in the calculation because small crystals were expected in copolymers with high comonomer content. However, for **v** greater than 100, this term was negligible and was therefore omitted from the calculations. It could not be assumed that the surface energy was the same for all crystals. The large range in melting temperatures probably resulted from the combined effects of variations in crystal thickness and variations in

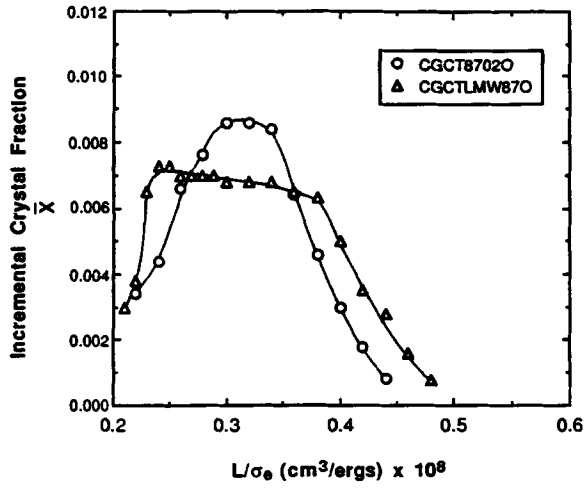

Figure 10 Incremental crystal fraction ($\bar{\mathbf{X}}$) of (△) CGCTLMW87-O and (○) CGCT8702-O.

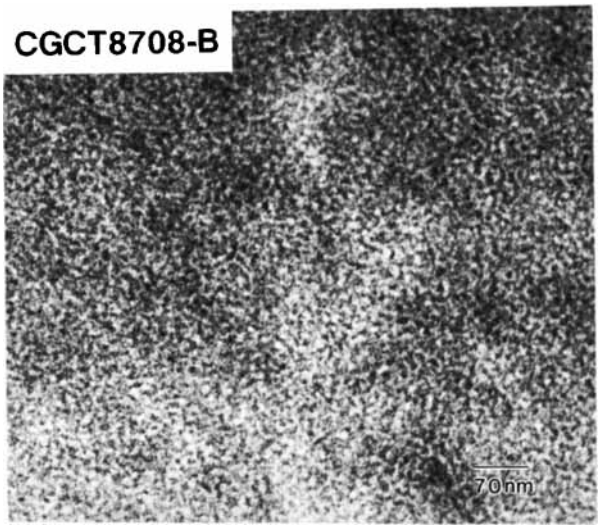

Figure 11 A thin section of CGCT8708-B cooled at 15°C/min.

surface energy as determined by the surface ordering. The terms **L** and σ_e appear in eq. (1) as a ratio:

$$\frac{\mathbf{L}}{\sigma_e} = \frac{2}{\Delta H_m^0}\left[1 - \frac{T_m}{T_m^0}\right]^{-1} \quad (2)$$

To calculate the ratio from eq. (2), the annealing temperature was taken as the melting temperature. The cumulative crystallinity **X** is plotted vs. $\mathbf{L}/\sigma_e$ in Figure 6(b) for the copolymers with the lowest and the highest density.

The derivative of the cumulative crystallinity with respect to T_m yields an incremental crystal

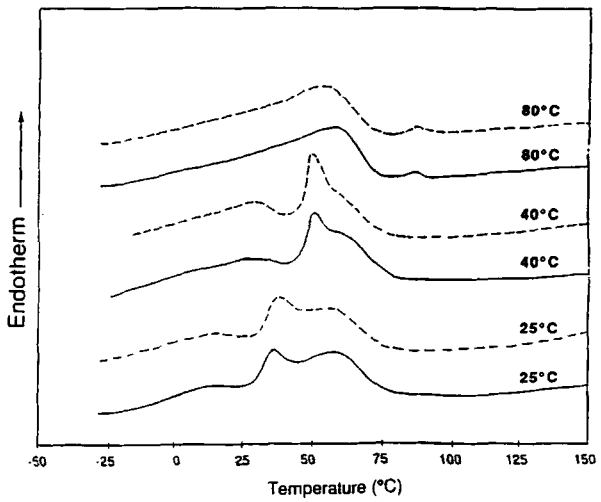

Figure 12 Selected thermograms of annealed (----) CGCT8708-B (I_2 = 0.8) and (———) CGCT8702-O (I_2 = 0.8). The annealing temperature (T_a) is indicated.

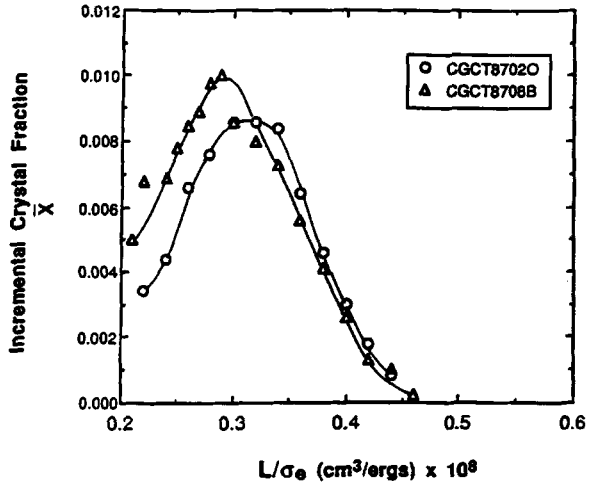

Figure 13 Incremental crystal fraction ($\bar{\mathbf{X}}$) of (△) CGCT8708-B and (○) CGCT8702-O.

fraction $\bar{\mathbf{X}}$ that more clearly reveals differences in the melting behavior of the copolymers. When $\bar{\mathbf{X}}$ is plotted as a function of $\mathbf{L}/\sigma_e$ (Fig. 7), the CGCT863-O copolymer shows a single peak, compared to CGCT9016-O, which has two peaks, a smaller one close to that of CGCT863-O and a larger peak at a higher $\mathbf{L}/\sigma_e$ ratio. The plots for the two copolymers with intermediate densities are included in Figure 7. The CGCT8702-O copolymer has a single peak at about the same $\mathbf{L}/\sigma_e$ ratio as does CGCT863-O. On the other hand, CGCT8817-O resembles CGCT9016-O with two peaks. The smaller peak is at about the same $\mathbf{L}/\sigma_e$ ratio as the single peak of the lower-density copolymers. The larger peak is at a somewhat lower $\mathbf{L}/\sigma_e$ ratio than is the larger peak of CGCT9016-O.

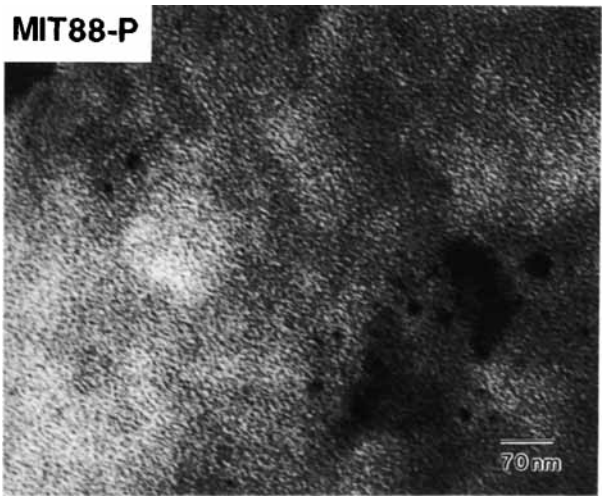

Figure 14 A thin section of slowly cooled MIT88-P.

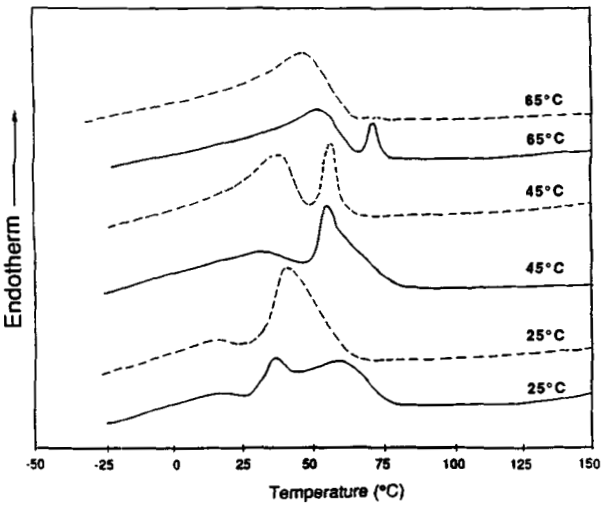

Figure 15 Selected thermograms of annealed (----) MIT88-P (I_2 = 1.1) and (———) CGCT8702-O (I_2 = 0.8). The annealing temperature (T_a) is indicated.

The $\mathbf{L}/\sigma_e$ ratio is a measure of the combined effects of comonomer on crystal thickness and surface order. When there are two peaks, it suggests that there are two crystal populations: a more ordered population with a higher $\mathbf{L}/\sigma_e$ ratio and a less ordered population with a lower $\mathbf{L}/\sigma_e$ ratio. An obvious approach is to identify the two populations as lamellar crystals and bundled crystals. The morphological observations tend to support this interpretation: CGCT9016-O has two $\mathbf{L}/\sigma_e$ peaks and micrographs of slowly cooled CGCT9016-O reveal both lamellar and bundled crystals. Conversely, CGCT863-O and CGCT8702-O have a single $\mathbf{L}/\sigma_e$ peak and micrographs exhibit only the features of bundled crystals.

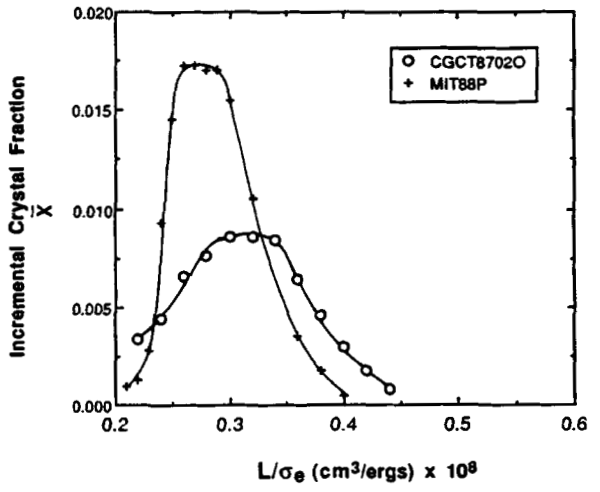

Figure 16 Incremental crystal fraction ($\bar{\mathbf{X}}$) of (+) MIT88-P and (O) CGCT8702-O.

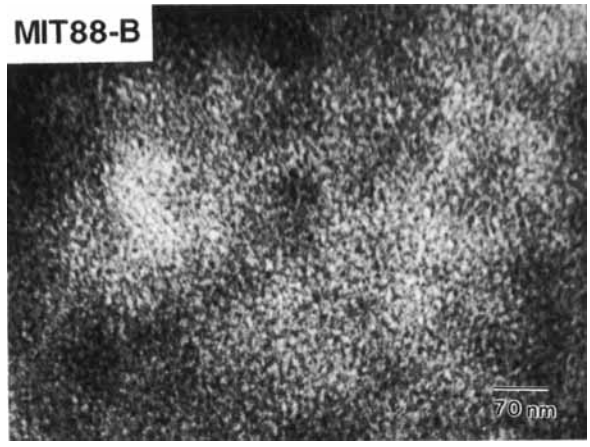

Figure 17 A thin section of slowly cooled MIT88-B.

Molecular Weight and Comonomer-type Effects

The effect of molecular weight was examined with two copolymers of approximately the same density, 0.87 g/cc, but different melt flow indices. A thin section taken from a rapidly cooled sample of CGCTLMW87-O shows almost the same morphological features as those of CGCT8702-O (Fig. 8). The overall texture is granular and often the granules are aligned in beaded strings about 75–100 Å thick. In places, the strings are arranged in small stacks. The short, unbeaded segments resembling lamellar fragments that appeared in micrographs of CGCT8702-O are not seen in the lower molecular weight sample.

Selected thermograms from annealed samples of CGCT8702-O (MI = 0.8) and CGCTLMW87-O (MI = 80) are compared in Figure 9. The thermograms

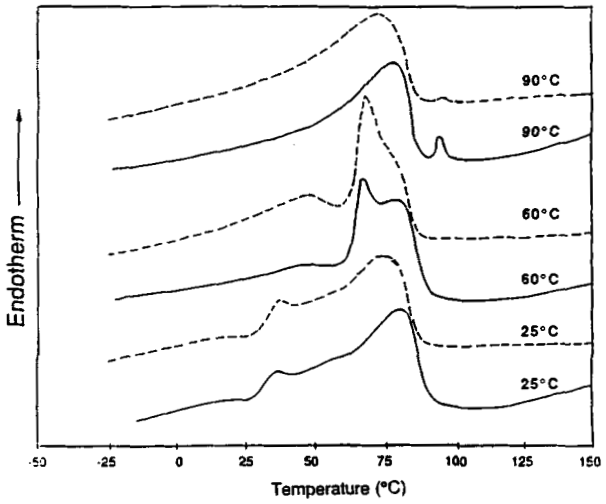

Figure 18 Selected thermograms of annealed (----) MIT88-B (I_2 = 3.6) and (———) CGCT8817-O (I_2 = 0.9). The annealing temperature (T_a) is indicated.

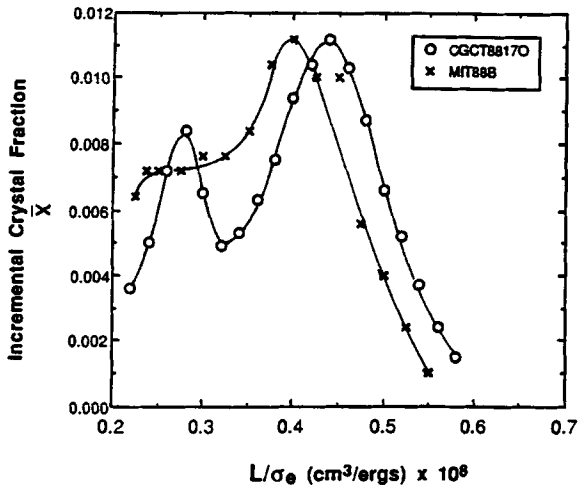

Figure 19 Incremental crystal fraction ($\bar{X}$) of (x) MIT88-B and (O) CGCT8817-O.

are basically the same except for slight differences in the size of the second endotherm above T_a. The total crystallinity is about 15% for both copolymers. The subtle differences are brought out when the incremental crystallinity is plotted as a function of $\mathbf{L}/\sigma_e$ (Fig. 10). Although both copolymers exhibit a single peak centered at the same $\mathbf{L}/\sigma_e$ ratio, the peak is much broader for the low molecular weight copolymer and includes crystals with larger and smaller $\mathbf{L}/\sigma_e$ values. If the distribution of ethylene sequence lengths is similar in the two copolymers, the broader distribution in $\mathbf{L}/\sigma_e$ of CGCTLM87-O can be attributed to easier diffusion of the shorter chains to the crystal front.

The morphology of CGCT8708-B, a butene copolymer with the same molecular weight and density as that of CGCT8702-O, is shown in Figure 11. As in the octene copolymer, there are numerous stacks of beaded strings 75–100 Å in thickness. The absence of the occasional short, unbeaded string segment that resembles a lamellar fragment is the only morphological difference between the two copolymers. This is probably a consequence of shorter ethylene sequences in the butene copolymer. About 20% more comonomer on a molar basis is needed to achieve a CGCT butene copolymer with the same density as that of the CGCT octene copolymer. Consequently, there are not as many of the longer ethylene sequences, which are the ones that would form the lamellar fragments.

The thermograms of the annealed samples are very similar in both peak positions and relative intensities (Fig. 12). The only discernible difference is the slightly smaller high-temperature endotherm in the butene copolymer. When the incremental crystallinities of the octene and butene copolymers are compared (Fig. 13), a single peak is seen for both; however, the peak occurs at a slightly lower value of $\mathbf{L}/\sigma_e$ for CGCT8707-B. This is consistent with the higher comonomer content and shorter ethylene sequences in the butene copolymer.

Comparisons were also made with copolymers of similar densities polymerized with a different catalyst system. The comonomer distribution might be more blocky in these copolymers, which would result in long ethylene sequences and sharper melting endotherms. Additionally, the propylene copolymer (MIT88-P) has methyl branches which may be incorporated into the polyethylene crystal. Consequently, a much higher mol % of propylene is needed to achieve the same density as that of an octene copolymer. A thin section taken from a slowly cooled sample of MIT88-P is shown in Figure 14. Compared to the octene copolymer of similar density, CGCT8702-O, there were fewer beaded strings in the propylene copolymer and these were slightly thinner (70 Å), stacking of the beaded strings occurred less frequently, and none of the unbeaded, lamellarlike fragments were visible.

Table III Crystal Thickness and Surface Energy Estimated from the Incremental Crystallinity ($\bar{X}$)

	Peak 1		Peak 2	
Copolymer	L (Å)	σ_e (erg/cm^2)	L (Å)	σ_e (erg/cm^2)
CGCT9016-O	75–100	214–286	140	233
CGCT8817-O	75–100	268–357	100	227
CGCT87LMW-O	75–100	313–417	—	—
CGCT8702-O	75–100	234–313	—	—
CGCT8708-B	75–100	268–357	—	—
CGCT863-O	100–130	357–464	—	—
MIT88-B	75–100	268–357	100	250
MIT88-P	75–100	288–385	—	—

The total crystallinity of MIT88-P, 17%, is only slightly higher than that of CGCT8702-O. However, the endotherms of MIT88-P do not extend to as high a temperature as those of CGCT8702-O (Fig. 15). Melting of MIT88-P is complete at 65°C, 15°C lower than complete melting of CGCT8702-O. As a consequence, a second melting peak above the annealing temperature is often not observed in thermograms of annealed MIT88-P. The narrower melting range of MIT88-P is reflected in the plot of incremental crystal fraction (Fig. 16). The single peak for MIT88-P is sharper and is at a lower $\mathbf{L}/\sigma_e$ ratio.

A similar comparison was made between a butene copolymer, MIT88-B, and the octene copolymer, CGCT8817-O, with the same density and the same crystallinity of 25%. A section of a slowly cooled MIT88-B sample in Figure 17 shows numerous short strings 75–100 Å thick. Occasionally, short segments of strings are not beaded. In terms of morphology, slowly cooled MIT88-B more closely resembles the lower-density, lower-crystallinity CGCT8702-O than it does CGCT8817-O.

Thermograms of annealed MIT88-B and CGCT8817-O, however, are quite similar (Fig. 18). Both copolymers when annealed at 25 and 60°C have two endotherms above T_a; the high-temperature endotherm is at a slightly lower temperature for MIT88-B. Instead of two distinct peaks in the incremental crystal fraction, as for CGCT8817-O, MIT88-B has a single peak with a shoulder (Fig. 19). The peak is at a slightly lower $\mathbf{L}/\sigma_e$ ratio than is the larger peak of CGCT8817-O; the shoulder is in the same $\mathbf{L}/\sigma_e$ range as the smaller peak of CGCT8817-O.

The effects of comonomer on crystal thickness and surface order are combined in the $\mathbf{L}/\sigma_e$ ratio; an independent measure of $\mathbf{L}$ would make it possible to estimate the surface energy term. Thickness measurements from micrographs are at best estimates; for example, the effect of thermal history on crystal thickness of copolymers with the bundled crystal morphology cannot be discerned in micrographs although the annealing experiments clearly show the existance of such an effect. Nevertheless, it seems reasonable to use approximate $\mathbf{L}$ values from the micrographs to obtain rough estimates of σ_e; these are tabulated in Table III. The values are considerably higher than those generally cited for regular folding, which are on the order of 100 erg/cm^2 (Ref. 20), but are closer to the range cited for bundled crystals, at least 300 erg/cm^2.[21] In comparing octene copolymers of similar molecular weight, the trend for the surface energy to increase as the comonomer content increases is reasonable. If the two $\mathbf{L}/\sigma_e$ peaks of CGCT9016-O are assigned to the two crystal populations in the micrographs, the surface energies calculated for lamellar crystals and bundled crystals are virtually the same. This would suggest that even when the copolymers crystallize in the form of lamellar crystals they do not possess a high degree of regular folding.

CONCLUSIONS

There is ample evidence from DSC that even in the lowest-density CGCT copolymers the bundled crystals recrystallize during isothermal annealing. Because it is likely that this also occurs during the DSC heating scan, it is not possible to relate the crystal thickness distribution calculated from the DSC endotherm to the crystal thickness distribution at ambient temperature unambiguously. An alternative approach in which copolymers are isothermally annealed at temperatures within the melting range was used to estimate the crystal distribution in CGCT copolymers with densities in the range 0.86–0.90 g/cc.

The results provide a clear distinction between Type I and Type II copolymers and, in this regard, strengthen the classification of CGCT ethylene–octene copolymers proposed previously.[4] Type I copolymers (density less than 0.89 g/cc) have a single-crystal population that is identified with the bundled crystals seen in transmission electron micrographs. A Type II copolymer (density of 0.90 g/cc) has two crystal populations that are identified, respectively, with lamellar crystals and bundled crystals. Although the morphology of a copolymer intermediate between Types I and II (density of 0.89 g/cc) consists of bundled crystals only, results of thermal analysis indicate that there is more than one crystal population.

Comparison of octene and butene copolymers of similar molecular weights and densities indicates that the crystal distribution of Type I copolymers is not strongly affected by the comonomer type. However, decreasing the molecular weight leads to a broader crystal distribution. Rough estimates of the surface energy suggest that even when the copolymers crystallize as lamellar crystals they do not possess a high degree of regular folding.

The financial support of The Dow Chemical Co. is gratefully acknowledged.

REFERENCES

1. K. Sehanobish, R. M. Patel, B. A. Croft, S. P. Chum, and C. I. Kao, *J. Appl. Polym. Sci.*, **51**, 887 (1994).

2. F. Defoor, G. Groeninckx, P. Schouterden, and B. Van der Heijden, *Polymer,* **33,** 3879 (1992).
3. F. Defoor, G. Groeninckx, P. Schouterden, and B. Van der Heijden, *Polymer,* **33,** 5186 (1992).
4. J. Minick, S. Bensason, A. Moet, A. Hiltner, E. Baer, and S. P. Chum, *J. Polym. Sci.: B: Polym. Phys.,* submitted.
5. Y.-C. Hwang, S. Chum, R. Guerra, and K. Sehanobish, *ANTEC 94 SPE Conf. Proceed.,* 3414 (1994).
6. V. B. F. Mathot, in *Calorimetry and Thermal Analysis of Polymers,* V. B. F. Mathot, Ed., Hanser, New York, 1994, Chap. 9.
7. O. Darras and R. Seguela, *Polymer,* **34,** 2946 (1993).
8. P. J. Mills and J. N. Hay, *Polymer,* **25,** 1277 (1984).
9. A. Wlochowicz and M. Elder, *Polymer,* **25,** 1268 (1984).
10. N. Alberola, J. Y. Cavaille, and J. Perez, *J. Polym. Sci. Polym. Phys. Ed.,* **28,** 569 (1990).
11. R. Alamo and L. Mandelkern, *J. Polym. Sci. Part B Polym. Phys.,* **24,** 2087 (1986).
12. L. Lu, R. G. Alamo, and L. Mandelkern, *Macromolecules,* **27,** 6671 (1994).
13. E. Adisson, M. Ribeiro, A. Deffieux, and M. Fontanille, *Polymer,* **33,** 4337 (1992).
14. S. Lai and G. W. Knight, *ANTEC 93 SPE Conf. Proceed.,* 1188 (1993).
15. B. Wunderlich, *Macromolecular Physics,* Academic Press, New York, 1980, Vol. 3, p. 42.
16. D. Montezinos, B. G. Wells, and J. L. Burns, *J. Polym. Sci. Polym. Lett. Ed.,* **23,** 421 (1985).
17. D. L. Wilfong and G. W. Knight, *J. Polym. Sci. Polym. Phys. Ed.,* **28,** 861 (1990).
18. P. H. Geil, *Polymer Single Crystals,* Wiley-Interscience, New York, 1963, Chap. 6.
19. D. Turnbull and R. L. Cormia, *J. Chem. Phys.,* **34,** 820 (1961).
20. F. C. Frank and M. Tossi, *Proc. R. Soc. Lond. A,* **263,** 323 (1961).
21. H. G. Zachmann, *Pure Appl. Chem.,* **38,** 79 (1974).

Received March 21, 1995
Accepted May 11, 1995